



**HAL**  
open science

# Efficient Real-Time Road Curvature Estimation : Visual-Inertial Approach

Obaida Alrazouk, Amine Chellali, Lamri Nehaoua, Hichem Arioui

► **To cite this version:**

Obaida Alrazouk, Amine Chellali, Lamri Nehaoua, Hichem Arioui. Efficient Real-Time Road Curvature Estimation: Visual-Inertial Approach. The 22nd World Congress of the International Federation of Automatic Control (IFAC 2023), Jul 2023, Yokohama, Japan. pp.4953–4958, 10.1016/j.ifacol.2023.10.1270 . hal-04068430

**HAL Id: hal-04068430**

**<https://hal.science/hal-04068430>**

Submitted on 13 Apr 2023

**HAL** is a multi-disciplinary open access archive for the deposit and dissemination of scientific research documents, whether they are published or not. The documents may come from teaching and research institutions in France or abroad, or from public or private research centers.

L'archive ouverte pluridisciplinaire **HAL**, est destinée au dépôt et à la diffusion de documents scientifiques de niveau recherche, publiés ou non, émanant des établissements d'enseignement et de recherche français ou étrangers, des laboratoires publics ou privés.

# Efficient Real-Time Road Curvature Estimation : Visual-Inertial Approach

Obaida Alrazouk<sup>\*</sup>, Amine Chellali<sup>\*</sup>, Lamri Nehaoua<sup>\*</sup>  
and Hichem Arioui<sup>\*</sup>

<sup>\*</sup> *Laboratoire IBISC, Université Paris-Saclay, Evry-Courcouronnes,  
France (e-mail: obaida.alrazouk@univ-evry.fr)*

---

## Abstract:

Road curvature is an essential parameter of road geometry, and it is crucial to set vehicle design and operating speeds. It can be utilized to identify the maximum stable velocity of a Powered Two Wheeled Vehicle (P2WV) and predict other safety-related events, including Lane departure and lane crossing. This paper proposes a new vision-based approach to estimate the road's curvature accurately and efficiently under real-time constraints for P2WV. The proposed method is based on the vanishing point approach to estimate the relative heading and its dynamics. Combined with the available vehicle speed and the yaw rate given by the inertial measurement unit (IMU), the instantaneous curvature of the road is reconstructed. The proposed algorithm is then tested using various simulated scenarios of different speeds and curvatures to validate the approach. Then it was compared to other estimation methods based on Inverse Perspective Mapping (IPM) to investigate the validity and efficiency in all scenarios regarding accuracy and time complexity. The proposed method shows very promising results in terms of error and real-time execution.

---

## 1. INTRODUCTION

Road safety has improved significantly during the past decades, thanks to higher quality training programs that have produced more qualified drivers on roads and increased adoption of driver's assistance and warning systems. In particular, Powered Four-Wheeled Vehicles (P4WV) have been gradually equipped with Advanced Driver Assistance Systems (ADAS), many of which have become required by law (e.g., Electronic Stability Control, Anti-lock Braking System, airbag systems).

Despite these improvements, little has been done for P2WV. Riders are still among the most vulnerable road users. A study published in 2019 ONISR (2019) shows that P2WV crashes are 22 times more fatal than P4WV, accounting for 23% of all traffic fatalities. Most P2WV crashes are due to problems when maneuvering curves.

For a novice driver, negotiating a bend in P2WV can be very complicated. The rider must adapt his speed to the geometry of the road, anticipate his trajectory, and carry out the vehicle's movement. The slightest error may lead to a fall. Even for expert riders, bends are high-risk areas due to inappropriate speeds or poor road conditions.

Schneider et al. (2010) and Clarke et al. (2004) conducted studies concerning the influence of road geometry on P2WV accidents. They clearly showed that curvature impacts the frequency and severity of P2WV accidents. They point out that 15% of all fatal P2WV accidents take place in bends for riders who are, in general, inexperienced. Among the factors involved, the authors identify the radius of the road curvature. It seems evident that adequate driver assistance systems could significantly contribute to reducing the number of P2WV accidents when cornering.

When cornering, the rider is supposed to anticipate the trajectory to perceive and decipher all the relevant safety cues. In addition to safety requirements, such as maintaining the traffic lane, it is necessary to consider the possibility of adapting the trajectory by narrowing it or widening it to avoid possible obstacles on the roadway. Therefore, the road's curvature determines the maximum safe speed to execute a maneuver.

Vision-based techniques to estimate road curvature have existed for a while. They all rely on the detection of lane markers. In the early 1980s, Dickmanns and Zapp (1987) proposed the first idea of using the extra information from the road lane markers to reconstruct the road curvature, vehicle's lateral offset, and relative heading using vision. After that, several algorithms have been developed using monocular cameras Pomerleau (1995) or stereo vision systems Bertozzi and Broggi (1998), region-based Alvarez and Lopez (2008), feature-based Liu et al. (2008), and spline fitting Wang et al. (2000) and Kim (2006). However, since all these methods were developed with a P4WV in mind, they relied on IPM to achieve a bird's eye view (BEV) of the road and then recover the lanes under the assumption of negligible roll dynamics.

However, these methods suffer from some problems. The limitation on the vehicle speed and the need for a road model, which are mostly assumed circular ignoring the change in curvature. Which sometimes could be significant. In addition, most of these approaches also rely on the assumption of a negligible roll angle. This assumption does not hold for P2WV as the rolling dynamics are significant, and thus making the IPM requires extra information about the roll angle based on inertial measurements. Estimating angles using an IMU sensor is vulnerable to drift errors.

Regarding curvature estimation, only a few studies have been done using a motorcycle. However, in a recent work, Damon et al. (2018) built on Dickmanns findings and extended to motorcycles to estimate the lateral offset, relative heading, and road curvature, taking into account the roll motion of the vehicle. However, the results for the curvature had large errors, despite assuming that the IMU provides a perfect angular position.

To solve this problem, a model-free, real-time, vision-based technique is proposed using a monocular camera aided with angular rates reading from the IMU to accurately estimate the curvature without needing a road model. First, the lane markers are detected, each fitted to a line, then the vanishing point of these lines is calculated, then the relative heading is estimated. After that, the relative heading rate is combined with the vehicle yaw rate to estimate the road's curvature more precisely.

## 2. DEFINITION AND OVERVIEW

Consider the case of a P2WV with a monocular camera traveling on a curved planar road under the assumption of visible lane markers. Let  $\mathcal{R}_w$  the world inertial frame.  $\mathcal{R}_o$  is the ground reference frame, where the  $x, y$  axes are in the plane of the road and its  $z$ -axis is upwards. This frame follows the road lane marker as its  $x$ -axis is always tangent to the lane marker.  $\mathcal{R}_v$  is the vehicle body frame, defined at the front wheel contact point when there is no steering.  $\mathcal{R}_{cs}$  is the camera frame which results from rotating  $\mathcal{R}_v$  around its  $y$ -axis with a known fixed angle  $\mu$ . Let  $\mathcal{R}_{cp}$  be another camera frame that follows the pinhole camera frame definition, where its origin is the optical point, its  $z$ -axis is the optical axis. Its  $x$  and  $y$  axes are the same orientation of the image's plane  $x$  and  $y$  directions, and finally, let  $\mathcal{R}_{ocp}$  be a local reference frame where its  $z$ -axis is always a tangent to the road lane marker, its  $x$ -axis is perpendicular to the lane marker to the inside of the road, and its  $y$ -axis is pointing downwards. It can be seen easily that the rotation matrix from  $\mathcal{R}_{ocp}$  to  $\mathcal{R}_o$  and from  $\mathcal{R}_{cp}$  to  $\mathcal{R}_{cs}$  are given by:

$${}^o\mathbf{R}_{ocp} = {}^{cs}\mathbf{R}_{cp} = \begin{bmatrix} 0 & 0 & 1 \\ -1 & 0 & 0 \\ 0 & -1 & 0 \end{bmatrix} \quad (1)$$

The last two reference frames are defined in this way to facilitate the estimation of the yaw angle.  $\psi_k$  is the relative heading angle between the vehicle heading and the  $x$ -axis of  $\mathcal{R}_o$ .  $v$  is the vehicle velocity at  $C$ .  $\psi_{tan}$  is the angle between  $x_o$  and  $x_w$ , and  $\psi_v$  is the vehicle's yaw angle.  $v$  is the velocity value, and  $v_x$  is the longitudinal velocity. Figures 1 and 2 illustrate the frames.

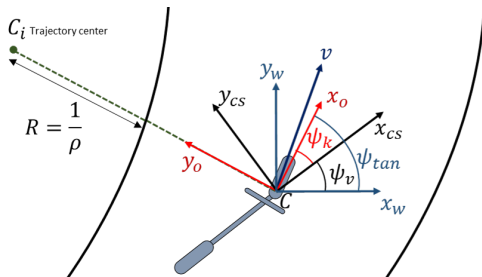


Fig. 1. P2WV on a curved road, frames definition-Top view

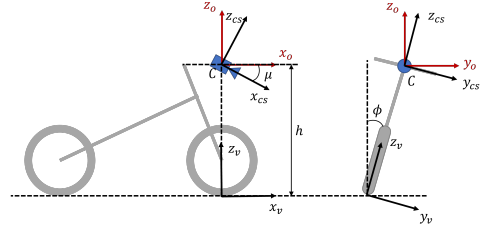


Fig. 2. P2WV on a curved road, with frames definition

Based on that definition, it can be shown that:

$$\psi_k = \psi_{tan} - \psi_v \quad (2)$$

Taking the derivative of equation (2) and dividing by  $v_x$ :

$$\frac{\dot{\psi}_k}{v_x} = \frac{\dot{\psi}_{tan}}{v_x} - \frac{\dot{\psi}_v}{v_x} \quad (3)$$

Under the assumption of near steady turning, one can estimate the curvature of the road as:

$$\rho = \frac{\dot{\psi}_{tan}}{v_x} \quad (4)$$

Substituting equation (4) in (3) and isolating  $\rho$  gives:

$$\rho = \frac{\dot{\psi}_k + \dot{\psi}_v}{v_x} \quad (5)$$

By approximating the value of  $v_x$  by  $v$ :

$$\rho = \frac{\dot{\psi}_k + \dot{\psi}_v}{v} \quad (6)$$

Assuming the knowledge of  $v$  and  $\dot{\psi}_v$ , which is outputted by the IMU,  $\dot{\psi}_k$  is the only one left to recover the curvature. The latter actually can be estimated using vision.

## 3. ESTIMATING RELATIVE HEADING AND ITS DERIVATIVE

### 3.1 Estimating pan angle from a vanishing point

Vanishing point detection is widely used in the literature to calibrate or recover the camera's pose. A vanishing point is where the perspective projections of parallel lines intersect, defining a point at infinity at real-world coordinates.

For a pinhole camera, the equation of perspective projection in the homogeneous coordinates is as follows:

$$s \cdot \begin{bmatrix} u \\ v \\ 1 \end{bmatrix} = \mathbf{K} \times [{}^{cp}\mathbf{R}_{ocp} | \mathbf{t}] \times \begin{bmatrix} X \\ Y \\ Z \\ 1 \end{bmatrix} \quad (7)$$

Where  $u, v$  are the pixel coordinates, and  $X, Y, Z$  are the coordinates in camera frame in meters,  $\mathbf{K}$  is the 3x3 calibration matrix,  ${}^{cp}\mathbf{R}_{ocp}$  is the 3x3 rotation matrix,  $\mathbf{t}$  is the translation vector between  $\mathcal{R}_{cp}$  and  $\mathcal{R}_{ocp}$ .

The interest is to find the vanishing point where the two road lanes intersect, which is in the  $z$  direction in the road frame  $\mathcal{R}_{ocp}$ . This vanishing point is expressed in the homogeneous coordinate system as

$$\mathbf{V}_z = [0 \ 0 \ 1 \ 0]^T \quad (8)$$

The zero at the last component indicates that the point lies at infinity. Assuming that  $\mathbf{v}_{pix}$  is the coordinates in pixel of the vanishing point in the image plane:

$$\mathbf{v}_{pix} = \mathbf{K} \times [{}^{cp}\mathbf{R}_{ocp}|\mathbf{t}] \times [0 \ 0 \ 1 \ 0]^T \quad (9)$$

which leads to

$$\mathbf{v}_{pix} = \mathbf{K} \times \mathbf{r}_3. \quad (10)$$

Where  $\mathbf{r}_3$  is the  $3^{rd}$  column of the rotation matrix  ${}^{cp}\mathbf{R}_{ocp}$ , knowing that  $\mathbf{r}_3$  should have a unit length:

$$\mathbf{r}_3 = \frac{\mathbf{K}^{-1} \times \mathbf{v}_{pix}}{\|\mathbf{K}^{-1} \times \mathbf{v}_{pix}\|} \quad (11)$$

However,  $\mathbf{r}_3$  can be expressed using pan and tilt angles only ( $\alpha, \beta$  respectively) as:

$$\begin{bmatrix} \sin \alpha \cdot \cos \beta \\ -\sin \beta \\ \cos \alpha \cdot \cos \beta \end{bmatrix} = \frac{\mathbf{K}^{-1} \times \mathbf{v}_{pix}}{\|\mathbf{K}^{-1} \times \mathbf{v}_{pix}\|} \quad (12)$$

Because of the way the camera is defined, it is only possible to get the last row of the rotation matrix  ${}^{cp}\mathbf{R}_{ocp}$  from the vanishing point. In order to estimate pan and tilt, a representation that enables to calculate the two angles just from the last column has to be chosen. Thus the use of the  $YXZ$  Euler representation, where the rotation matrix takes the following form:

$${}^{cp}\mathbf{R}_{ocp} = \begin{bmatrix} c_\alpha c_\gamma + s_\alpha s_\beta s_\gamma & c_\gamma s_\alpha s_\beta - c_\alpha s_\gamma & s_\alpha c_\beta \\ c_\beta s_\gamma & c_\beta c_\gamma & -s_\beta \\ -c_\gamma s_\alpha + c_\alpha s_\beta s_\gamma & c_\alpha c_\gamma s_\beta + s_\alpha s_\gamma & c_\alpha c_\beta \end{bmatrix} \quad (13)$$

Where  $s_\theta$  is  $\sin \theta$ , and  $c_\theta$  is  $\cos \theta$ . It can be seen that the last column is just composed of the pan and tilt angles. From this, the connection between the vanishing point and the pan and tilt angles can be concluded:

$$\mathbf{r}_3 = \begin{bmatrix} \sin \alpha \cdot \cos \beta \\ -\sin \beta \\ \cos \alpha \cdot \cos \beta \end{bmatrix} \quad (14)$$

Which gives the equations of both  $\alpha$  and  $\beta$  as follows:

$$\alpha = \text{atan2}(\mathbf{r}_3(1), \mathbf{r}_3(3)), \beta = -\text{asin}(\mathbf{r}_3(2)) \quad (15)$$

where  $\mathbf{r}_3(1), \mathbf{r}_3(2), \mathbf{r}_3(3)$  are the components of  $\mathbf{r}_3$ . However, these pan and tilt angles are represented in  $YZX$  Euler representation as seen in the next section, not the standard  $ZYX$  representation of interest.

### 3.2 From $YZX$ to $XYZ$ Euler representation

It can be shown that  $\alpha$  is exactly the yaw angle of  $\mathcal{R}_{cs}$  from  $\mathcal{R}_o$ , and  $\beta$  is the pitch angle of the frame  $\mathcal{R}_{cs}$  from  $\mathcal{R}_o$  following an  $XYZ$  Euler angles representation. In order to prove that  $\alpha$  and  $\beta$  are the yaw and pitch angles in  $XYZ$  representation,  ${}^o\mathbf{R}_{cs}$  need to be written in terms of  $\alpha$  and  $\beta$  and compare it with the rotation matrix in the  $XYZ$  convention. Starting from  ${}^{cp}\mathbf{R}_{ocp}$  as illustrated in equation (13), it can be found that:

$${}^o\mathbf{R}_{cs} = {}^o\mathbf{R}_{ocp} \times {}^{ocp}\mathbf{R}_{cp} \times {}^{cp}\mathbf{R}_{cs} \quad (16)$$

Where  ${}^o\mathbf{R}_{ocp}$  is available from equation (14). Moreover, it is known that:

$${}^{ocp}\mathbf{R}_{cp} = {}^{cp}\mathbf{R}_{ocp}^T \quad (17)$$

Substituting (14) and (17) in (16) results in:

$${}^o\mathbf{R}_{cs} = {}^{cp}\mathbf{R}_{cs}^T \times {}^{cp}\mathbf{R}_{ocp}^T \times {}^{cp}\mathbf{R}_{cs} \quad (18)$$

Furthermore, from (13) by substituting by values:

$${}^{cp}\mathbf{R}_{ocp} = \begin{bmatrix} c_\alpha c_\beta & -s_\alpha c_\beta & s_\beta \\ c_\gamma s_\alpha - c_\alpha s_\beta s_\gamma & c_\alpha c_\gamma + s_\alpha s_\beta s_\gamma & c_\beta s_\gamma \\ -c_\alpha s_\beta c_\gamma - s_\alpha s_\gamma & s_\alpha s_\beta c_\gamma - c_\alpha s_\gamma & c_\beta c_\gamma \end{bmatrix} \quad (19)$$

On the other hand, the rotation matrix constructed from the  $XYZ$  Euler convention can be given by:

$${}^o\mathbf{R}_{cs} = \mathbf{R}_x(-\phi) \times \mathbf{R}_y(\theta) \times \mathbf{R}_z(\psi) \quad (20)$$

By doing the matrices product, it can be shown that:

$${}^{cp}\mathbf{R}_{ocp} = \begin{bmatrix} c_\psi c_\theta & -s_\psi c_\theta & s_\theta \\ c_\phi s_\psi - c_\psi s_\theta s_\phi & c_\psi c_\phi + s_\psi s_\theta s_\phi & c_\theta s_\phi \\ -c_\psi s_\theta c_\phi - s_\psi s_\phi & s_\psi s_\theta c_\phi - c_\psi s_\phi & c_\theta c_\phi \end{bmatrix} \quad (21)$$

Since  $-\frac{\pi}{2} < \alpha, \beta, \gamma < \frac{\pi}{2}$  the rotation is unique, that means there is only one set of  $(\alpha, \beta, \gamma)$  that constructs this rotation, thus  $\psi = \alpha, \theta = \beta, \phi = \gamma$ . This proves that  $\alpha$  is indeed the yaw angle and  $\beta$  is the pitch angle of the camera in the  $XYZ$  Euler convention.

That proves that  $\alpha, \beta$  are the yaw and pitch of the camera in the  $XYZ$  representation. However, the interest is in the vehicle's relative yaw angle in  $ZYX$  representation.

### 3.3 From camera's yaw angle to vehicle's yaw angle

Writing the camera's rotation matrix starting from the vehicle's transformation matrix in  $ZYX$  representation:

$${}^o\mathbf{R}_{cs} = {}^o\mathbf{R}_v \times {}^v\mathbf{R}_{cp} \quad (22)$$

Which is equal to:

$${}^o\mathbf{R}_{cs} = \mathbf{R}_z(\psi_v) \times \mathbf{R}_y(\theta_v) \times \mathbf{R}_x(\phi_v) \times \mathbf{R}_y(\mu) \quad (23)$$

On the other hand, writing the rotation matrix of the camera in  $XYZ$  representation gives the following:

$${}^o\mathbf{R}_{cs} = \mathbf{R}_x(\phi_c) \times \mathbf{R}_y(\theta_c) \times \mathbf{R}_z(\psi_c) \quad (24)$$

Since the rotation matrix is the same regardless of the representation, the following can be written:

$$\mathbf{R}_z(\psi_v) \times \mathbf{R}_y(\theta_v) \times \mathbf{R}_x(\phi_v) \times \mathbf{R}_y(\mu) = \mathbf{R}_x(\phi_c) \times \mathbf{R}_y(\theta_c) \times \mathbf{R}_z(\psi_c) \quad (25)$$

The aim is to express  $\psi_v$  by only terms of  $\psi_c, \theta_c, \mu$ . However, this is not directly available from equation (25). Luckily, by utilizing a simple approximation of  $\theta_v \approx 0$  which translates to  $\cos \theta \approx 1, \sin \theta \approx 0$ , the matrix on the left side of (25) can be simplified. By taking the second column of both sides, it can be shown that:

$$\begin{bmatrix} c_{\theta_c} c_{\psi_c} \\ -c_{\theta_c} s_{\psi_c} \\ s_{\theta_c} \end{bmatrix} = \begin{bmatrix} c_\mu c_{\psi_v} - s_\mu s_{\phi_v} s_{\psi_v} \\ -c_{\phi_v} s_{\psi_v} \\ c_{\psi_v} s_\mu + c_\mu s_{\phi_v} s_{\psi_v} \end{bmatrix} \quad (26)$$

Which leads to:

$$\begin{bmatrix} c_{\theta_c} c_{\psi_c} - c_\mu c_{\psi_v} \\ c_{\theta_c} s_{\psi_c} \\ s_{\theta_c} - c_{\psi_v} s_\mu \end{bmatrix} = \begin{bmatrix} -s_\mu s_{\phi_v} s_{\psi_v} \\ c_{\phi_v} s_{\psi_v} \\ c_\mu s_{\phi_v} s_{\psi_v} \end{bmatrix} \quad (27)$$

By dividing the first row by the third in equation (27):

$$\frac{c_{\theta_c} c_{\psi_c} - c_\mu c_{\psi_v}}{s_{\theta_c} - c_{\psi_v} s_\mu} = \frac{-s_\mu}{c_\mu} \quad (28)$$

Which leads to the following equation:

$$\cos \psi_v = \frac{\cos \theta_c \cos \psi_c + \tan \mu \sin \theta_c}{\tan \mu \sin \mu + \cos \mu} \quad (29)$$

Using equation (29) it is possible to recover the value of the required angle. However, it is known that arccos does not recover the sign. To recover the sign of the angle, the second row from equation (27) can be used:

$$\text{sign}(\sin \psi_v \cos \phi_v) = \text{sign}(\cos \theta_c \sin \psi_c) \quad (30)$$

since  $-\frac{\pi}{2} < \phi_v, \theta_c < \frac{\pi}{2}$  that means that  $\cos \phi_v, \cos \theta_c > 0$ . Which translates to:

$$\text{sign}(\sin \psi_v) = \text{sign}(\sin \psi_c) \quad (31)$$

Which gives:

$$\text{sign}(\psi_v) = \text{sign}(\psi_c) \quad (32)$$

From (32) and (29), it can be concluded that:

$$\psi_k = \psi_v = \text{sign}(\psi_c) \arccos\left(\frac{\cos \theta_c \cos \psi_c + \tan \mu \sin \theta_c}{\tan \mu \sin \mu + \cos \mu}\right) \quad (33)$$

Before estimating the  $\psi_k$  rate, one should consider filtering  $\psi_k$  to remove the noise and smooth the function. A Gaussian average filter with a window size of the number of samples in a second is applied. After filtering, the derivative at sample  $n$  is estimated using the following:

$$\dot{\psi}_{k,n} = \frac{\psi_{k,n} - \psi_{k,n-1}}{t_n - t_{n-1}} \quad (34)$$

Where  $\psi_{k,n}$  is the estimated filtered relative heading at sample  $n$ , and  $t_n$  is the time at sample  $n$ .

### 3.4 Detecting the vanishing point

For detecting the pixel coordinates of the vanishing point, many methods exist in the literature Dixon et al. (2000) and Huang et al. (2014) but basically, they all rely on the same principle, detecting the lane edges (and other parallel lines) remove the outliers and find the intersecting point of these lines. The same basic idea is used assuming that the two edge lane markers are always visible to the camera, empty road, clear sky, and no strange objects nearby. First, the image is converted to a binary image through thresholding, then detecting connected components and filtering them out according to their size, then picking the left and right lanes, extracting one edge of each lane for the first few meters in front of the camera, fit each edge points with a line, then intersecting these two lines to detect the tangent point. Figure 3 illustrates these steps.

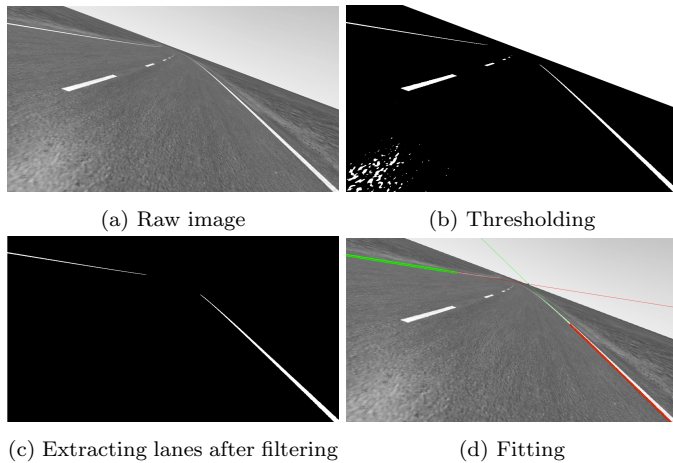


Fig. 3. Estimating relative heading- algorithm steps

## 4. SIMULATION RESULTS

The growth of computational power allowed to build, calculate, and simulate complex vehicle models. Advanced

simulator software that help simulate different scenarios are available cheaply, more conveniently, and accurately enough without experimenting on actual vehicles and with the ability to measure different variables by installing cameras and IMUs on a specific point. One of the most popular software to simulate P2WV is BikeSim, which is used here to create different driving scenarios. Several roads were constructed with known curvatures at each point and tested several scenarios with sections of low curvature, changing curvature, fixed curvature, and straight road. It is important to mention that the roads are planar, empty with a well-lit environment, and no strange objects in the scene. The camera was installed at the height of  $h = 1.1m$  and tilted  $\mu = 15^\circ$  in the virtual environment. The camera's resolution was (1080x720) at 60 FPS with a horizontal field of view of  $80^\circ$ . All these tests were carried out on a Matlab R2020b environment, installed on Windows 10, on a mid-range laptop with an AMD Ryzen 3750H chip.

### 4.1 Clothoid track

The clothoid track has varying curvature, so it is considered hard to estimate, especially at high speeds. Which is defined by  $C(l) = C_0 + C_1.l$  where  $C_0$  is the initial curvature,  $C_1$  is the curvature rate, and  $l$  is the curve length.

This part has been simulated at  $80km/h$ . The estimation of curvature for the clothoid is very good and accurate, as in figure 4.a, with an RMS value of  $1.1 * 10^{-4}[m^{-1}]$ . One important thing to note is that the estimation preserved the linearity of curvature change despite being very small.

### 4.2 Circular track

In this scenario, the circular track is a road with fixed curvature. Usually, it is not hard to estimate, but this becomes more difficult to estimate the lower the curvature and the higher the speed. Thus, estimating such a slight curvature of  $10^{-3}[m^{-1}]$  at high speed  $120km/h$  is very interesting because it assesses the algorithm's performance. The estimation of the slight curvature is also very good and accurate, as in figure 4.b, with an RMS value of  $2.3 * 10^{-5}[m^{-1}]$ .

### 4.3 Straight road

The straight line is technically the easiest for the algorithm and has a curvature of zero (infinite radius). The estimation of curvature for the clothoid is also very good, as in figure 4.c, with an RMS value of  $3.2 * 10^{-5}$ .

### 4.4 Complex track with multiple sections

This track represents a challenging scenario where the track is changing shape. It is constructed from several connected sections. Each section is a straight line, a circle, or a clothoid. The curvatures are high; this is why this scenario is done at a low speed of  $50km/h$ , which took approximately  $144 sec$  to achieve. In figure 4.d, the approximation is very accurate, with more significant errors on the points of discontinuity.

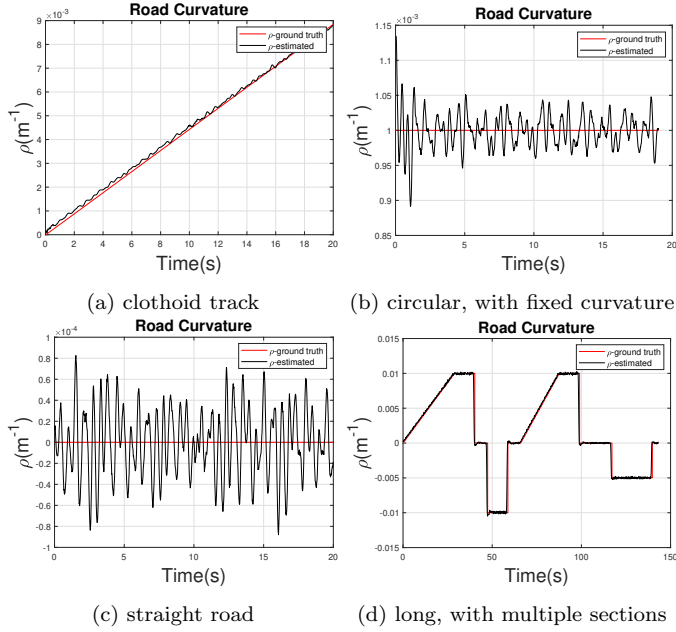


Fig. 4. Estimating curvature in various scenarios

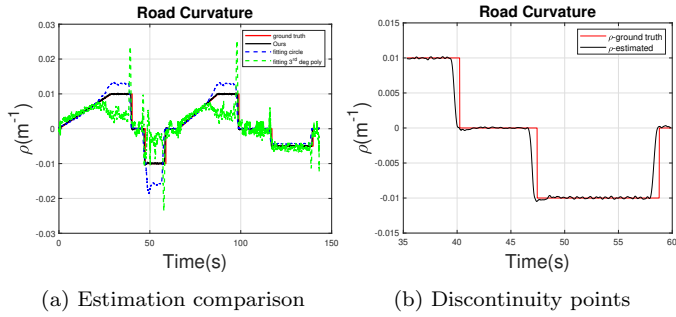


Fig. 5. Curvature estimation comparison using different methods and curvature discontinuity problem

#### 4.5 Comparison with the state of art

The most popular methods for curvature estimation are the ones that utilize the IPM technique. After doing the IPM, the lanes are fitted to a  $3^{rd}$  degree polynomial or a circle. A comparison between the proposed method, the  $3^{rd}$  degree polynomial fitting using IPM presented by Damon et al. (2018), and circle fitting presented by Pratt (1987), which also uses the least squared method to optimize for the curvature is presented in figure 5.a, and a comparison of errors of estimation, is provided in figure 6.d for the long multi-section track. The same dataset was fed to the three different algorithms to compare their accuracy. Table 1 demonstrates the RMSE of each method for all types of roads mentioned earlier. It is seen that the proposed method has orders of magnitude less error on clothoid and straight roads compared to the other methods. Figure 6.d illustrate the estimation error in each case.

In figure 5.a, the  $3^{rd}$  degree polynomial fitting is the least accurate. It suffers significantly on section change, clothoid section, and even on a circular section with fixed curvature. The circle fitting method performs better in general but also fails on the clothoid section and overshoots for circular sections. It can be clearly seen that the proposed method

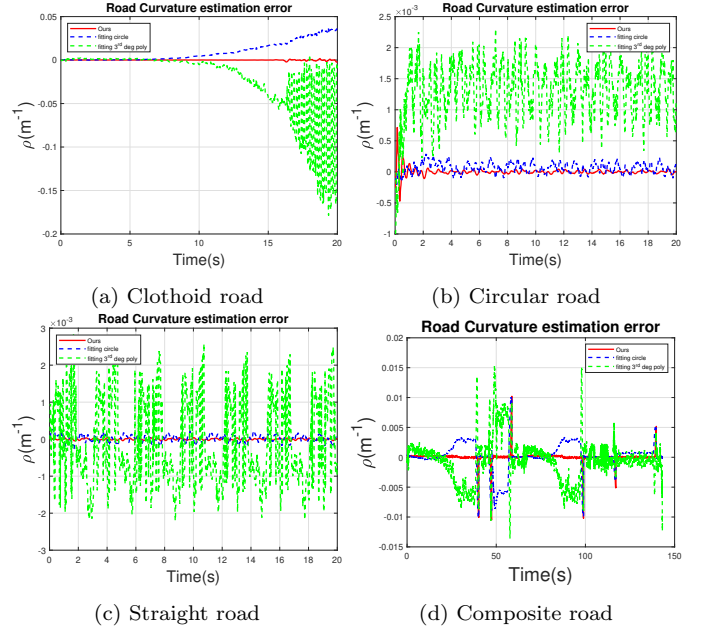


Fig. 6. Curvature error estimation in different scenarios

outperforms the other techniques significantly, plus it conserves the linear change of curvature for clothoid sections.

In addition, there is also a difference in performance. The proposed method can do a stable 120fps on the resolution of (1080x720), while the other two methods can only do a stable 60fps on the exact image resolution. This is because the IPM step is computationally expensive. Table 2 shows the maximum FPS that each method can perform.

Table 1. RMSE of curvature estimation in different scenarios for different methods

Scenario	IPM $3^{rd}$ deg poly fit [ $m^{-1}$ ]	IPM circle fit [ $m^{-1}$ ]	Proposed method [ $m^{-1}$ ]
Straight road	0.0011	7.70E-05	3.25E-05
Circular road	0.0014	1.04E-04	5.40E-05
Clothoid road	0.0438	0.0144	3.80E-04
Combined sections	0.0038	0.0025	0.0012

Table 2. FPS values for different methods

Method	IPM $3^{rd}$ deg poly fit	IPM circle fit	Proposed method
FPS (Hz)	77.4	78.5	135.3

## 5. DISCUSSION

As stated in the simulation section, the estimation is very close in all scenarios and performs better than the state of art that utilize IPM techniques in terms of accuracy and computation time. However, the approximation for the points of discontinuity for curvature is less accurate, as illustrated in figure 5.b, and as represented in sharp pulses of error in figure 6.d. The reason for this lies in the visual approach itself because the fitted lane markers are parts of the foreseen curvature, not the actual curvature at the motorcycle position, but the difference is very small

depending on how much distance ahead is captured by the camera. More precisely, the approximation of  $\psi_k$  from the vanishing point approach using vision relies on fitting the lane marker visible in the image, which is always a little ahead of the actual curve point assumed to be calculated. This effect can be dramatically reduced by using a large field of view camera.

As seen in table 1, the algorithm proves to be very accurate in all scenarios with very low RMSE values. It has orders of magnitude less error than the compared methods in clothoid and straight roads and half the error in the others. In addition, it preserves the linear change in curvature for a clothoid road. As seen from figure 5.a and 6.d, the proposed method performs significantly better than the other compared methods, At (1080x720), and as seen in table 2, the proposed method can perform twice as fast. It can do 135fps compared to the 78fps in IPM with circle fit and 77fps in IPM with 3<sup>rd</sup> degree polynomial. The main reason for the time complexity difference is the utilization of the computationally expensive IPM technique.

While increasing the image’s resolution will significantly improve the IPM-based methods, it has little to no effect on the proposed method because it relies on the calculation of the tangent point, which is done by intersecting the fitted lines to have sub-pixel coordinates of the intersection point. Increasing the resolution after a threshold will not change the equations for the fitted lines, thus the intersection point does not change. A primary disadvantage of the IPM-based techniques is the utilization of the roll angle, which suffers from drift due to the integration of the IMU roll rate. In comparison, the proposed method utilizes the yaw rate directly measured by the IMU, leading to no drift error.

## 6. CONCLUSION

Road curvature is a very important parameter for P2WV, as it can set the maximum safe speed and help predict lane departure and crossing. This work introduces a visual-inertial approach to estimate road curvature in real time. The advantage of this method is that it does not assume a road model, works on P2WV with significant rolling dynamics, and is faster than other IPM-based techniques.

Under the assumptions of a planar road, lane marks that are visible at all times, empty roads, and good lighting conditions, the proposed method can accurately estimate the instantaneous curvature of the road. For each image taken, the relative heading is estimated using the vanishing point approach by extracting the lane markers in the near vicinity and fitting them into straight lines, then intersecting these lines to have the vanishing point coordinates, which will give the relative heading. After that, the derivative of the relative heading is estimated and added to the yaw rate measured from the IMU. Combined with the velocity, the latter sum estimates the curvature.

The proposed method was tested on several simulated driving scenarios on different tracks, varying in difficulty and speed. It was able to estimate the curvature accurately. It was also compared using a long track with several sections of different curvatures to IPM-based techniques that use 3<sup>rd</sup> degree polynomial fit and circle fit to esti-

mate the lane markers curve in the image. The proposed method performed better than the others in every scenario, especially scenarios where the curvature is changing.

## 7. ACKNOWLEDGMENT

This work has been financially supported by projet ANR eMC2 number ANR-22-CE22-0012.

## REFERENCES

- Alvarez, J. and Lopez, A. (2008). Novel Index for Objective Evaluation of Road Detection Algorithms. In *2008 11th International IEEE Conference on Intelligent Transportation Systems*, 815–820. IEEE, Beijing, China.
- Bertozzi, M. and Broggi, A. (1998). GOLD: a parallel real-time stereo vision system for generic obstacle and lane detection. *IEEE Transactions on Image Processing*, 7(1), 62–81.
- Clarke, D., Ward, P., Bartle, C., and Truman, W. (2004). In-depth study of motorcycle accidents.
- Damon, P.M., Hadj-Abdelkader, H., Arioui, H., and Youcef-Toumi, K. (2018). Image-based lateral position, steering behavior estimation, and road curvature prediction for motorcycles. *IEEE Robotics and Automation Letters*, 3(3), 2694–2701.
- Dickmanns, E.D. and Zapp, A. (1987). A CURVATURE-BASED SCHEME FOR IMPROVING ROAD VEHICLE GUIDANCE BY COMPUTER VISION. In *Mobile robots : proceedings of SPIE*.
- Dixon, P., Best, M., and Gordon, T. (2000). An Extended Adaptive Kalman Filter for Real-time State Estimation of Vehicle Handling Dynamics. *Vehicle System Dynamics*, 34(1), 57–75.
- Huang, C., Chen, L., Jiang, H., Yuan, C., and Xia, T. (2014). Fuzzy chaos control for vehicle lateral dynamics based on active suspension system. *Chinese Journal of Mechanical Engineering*, 27(4), 793–801.
- Kim, Z. (2006). Realtime lane tracking of curved local road. In *2006 IEEE Intelligent Transportation Systems Conference*. IEEE.
- Liu, W., Zhang, H., Duan, B., Yuan, H., and Zhao, H. (2008). Vision-Based Real-Time Lane Marking Detection and Tracking. In *2008 11th International IEEE Conference on Intelligent Transportation Systems*, 49–54. IEEE, Beijing, China.
- ONISR (2019). La sécurité routière en France: Bilan de l’accidentalité de l’année 2019. Technical report, ONISR (Observatoire National Interministériel de la Sécurité Routière), Tech. Rep..
- Pomerleau, D. (1995). RALPH: rapidly adapting lateral position handler. In *Proceedings of the Intelligent Vehicles ’95. Symposium*, 506–511. IEEE, Detroit, MI, USA.
- Pratt, V. (1987). Direct least-squares fitting of algebraic surfaces. In *Proceedings of the 14th annual conference on Computer graphics and interactive techniques - SIGGRAPH ’87*. ACM Press.
- Schneider, W.H., Savolainen, P.T., and Moore, D.N. (2010). Effects of horizontal curvature on single-vehicle motorcycle crashes along rural two-lane highways. *Transportation Research Record: Journal of the Transportation Research Board*, 2194(1), 91–98.
- Wang, Y., Shen, D., and Teoh, E.K. (2000). Lane detection using spline model. *Pattern Recognition Letters*, 21(8), 677–689.